Energy and enstrophy transfer in numerical simulations of two-dimensional turbulence

Mathew E. Maltrud[a] and Geoffrey K. Vallis
University of California, Santa Cruz, Santa Cruz, California 95064

(Received 1 October 1992; accepted 25 March 1993)

Numerical simulations of statistically steady two-dimensional (2-D) turbulence are analyzed to determine the relative importance of the types of wave-vector triad interactions that transfer energy and enstrophy in the both the energy and enstrophy inertial ranges. In the enstrophy inertial range, it is found (in agreement with previous studies [J. Fluid Mech. **72**, 305 (1975); Phys. Fluids A **2**, 1529 (1990)]) that the important triads (i.e., those associated with the highest transfer rates) are typically very elongated. On the average, nearly all of the enstrophy transfer within these triads is directed from the intermediate to the largest wave-number mode (i.e., downscale transfer). Energy, too, is transferred downscale in this manner, but is also transferred upscale due to the interaction of the intermediate with the smallest wave-number mode of the triad, resulting in no net flux of energy in the enstrophy inertial range. Analysis of the geometry of the important triads indicates they are not of similar shapes at all scales, and that the enstrophy transferring triads generally consist of one wave vector near the scale of the energetic peak, no matter how large the other wave vectors are. In the energy inertial range, elongated triads are also important. As in the enstrophy inertial range, there is downscale transfer of energy and enstrophy due to the interaction of the intermediate with the largest wave-number mode. There is also upscale transfer of both energy and enstrophy due to a very nonlocal interaction involving the smallest wave-number modes. The result is a net upscale flux of energy and no net flux of enstrophy in the energy inertial range. Comparison of the transfer functions from the simulations with those calculated by an eddy-damped quasinormal closure show agreement in the gross functional forms, but display certain quantitative differences in integrated quantities such as total transfer into and flux past a given wave number.

I. INTRODUCTION

Inertial range theories are usually derived on the assumption that spectrally far away from the forcing and dissipation scales, the energy spectrum depends only on the cascade rate, the wave number k and a universal constant. Equivalently, interactions between different scales of motion are thought of as spectrally local; that is, only those interactions with wave numbers in the vicinity of wave number k are important. The locality assumption can be tested heuristically by considering the strain rate at k,

$$R(k)=\left(\int_0^k p^2E(p)dp\right)^{1/2}. \tag{1}$$

For a $k^{-5/3}$ spectrum, expected in three-dimensional turbulence and in the inverse cascade region of two-dimensional turbulence, the integral is dominated by contributions from around k, supporting the idea of locality. However, the k^{-3} spectrum expected in the enstrophy range of two-dimensional turbulence gives rise to equal contributions from all octaves of the spectrum, implying nonlocality. Such nonlocality is also present in the log-corrected spectrum of Kraichnan.[1] Thus, based on such heuristic arguments, Kolmogorovian theories of two-dimensional (2-D) turbulence appear to verge on the brink of self-inconsistency.

Numerical simulations of 2-D turbulence with forcing at large scales have in fact shown that long-lived coherent structures sometimes make up a significant fraction of the flow field,[2–4] and energy spectra from these simulations have slopes significantly steeper than k^{-3} for (at least) part of the enstrophy inertial range. Arguments based on (1) would then suggest that nonlocal interactions should indeed be important in this case. Simulations forced at small scales show a well-developed $k^{-5/3}$ energy inertial range[4,5] which, on the other hand, might be expected to be characterized by relatively local interactions. (See Ref. 6 for a review of current phenomenology.) In this paper, our goal is to go beyond such arguments by examining the behavior of actual triad interactions calculated by numerical simulations.

Most studies of transfer and fluxes in turbulent flows have thus far been performed using closure models, such as test field model (TFM)[7] and eddy-damped quasinormal Markovian (EDQNM)[8] studies. Ohkitani[9,10] has recently presented an investigation of transfer in numerical simulations of the 2-D enstrophy inertial range similar to part of the work presented here (specifically, portions of Sec. III), as well as an interesting analysis of spectral and real space transfer based on Weiss'[11] vorticity-strain decomposition

[a]Present address: Fluid Dynamics Group, MS B216, Los Alamos National Laboratory, Los Alamos, New Mexico 87545.

 0899-8213/93/5(7)/1760/16/$6.00

that attempts to isolate the effects of coherent structures on the transfer. These studies imply that interactions in the enstrophy inertial range involve elongated triads. Our study differs from and extends Ohkitani's in several respects: transfer in the inverse energy cascade is also analyzed, as are the fluxes in both inertial ranges, and we perform comparisons with an analytical closure model.

In any analysis of spectral transfer, it is important to distinguish between the locality of *interactions* and the locality of the actual *transfer*.[12] For example, we will find indeed that important inertial range triads are typically nonlocal, meaning that two of the legs are much longer than the third. This does not necessarily imply that the transfer is nonlocal; this depends on which members of the triad gain or lose significant energy or enstrophy. Another important distinction must be made between the transfer (or transfer rate) and the flux (or cascade rate). The transfer describes the time rate of change of energy or enstrophy in mode k, while the flux is the total amount of energy or enstrophy flowing *past* mode k: its divergence gives the transfer. These distinctions will become more clear as the results are presented.

II. FORMULATION

The model equation for this study of 2-D turbulence is the incompressible vorticity equation

$$\frac{\partial \zeta}{\partial t}+J(\psi,\zeta)=F+D, \tag{2}$$

where ψ is the streamfunction defined such that $\mathbf{u}=\hat{z}\times\nabla\psi$, $\zeta=\hat{z}\cdot\nabla\times\mathbf{u}=\nabla^2\psi$ is the relative vorticity, J is the two-dimensional Jacobian operator, $J(\psi,\zeta)\equiv\psi_x\zeta_y-\psi_y\zeta_x$, and F and D represent generic forcing and dissipation functions. We solve (2) in a doubly periodic domain. Hence, we may express the vorticity and streamfunction in terms of a complex Fourier series,

$$\psi(x,y)\equiv\sum_{\mathbf{k}=1}^{\mathbf{k}_{\max}}\psi_{\mathbf{k}}(t)e^{i\mathbf{k}\cdot\mathbf{x}}, \tag{3}$$

where $\psi_{\mathbf{k}}^*=\psi_{-\mathbf{k}}$ to ensure reality of the physical field, and $*$ denotes complex conjugacy. Then the equation of motion (2) takes the following form:

$$\dot{\zeta}_{\mathbf{k}}+J_{\mathbf{k}}=F_{\mathbf{k}}+D_{\mathbf{k}}, \tag{4}$$

where

$$J_{\mathbf{k}}=\sum_{\mathbf{pq}}a_{\mathbf{kpq}}\psi_{\mathbf{p}}^*\psi_{\mathbf{q}}^* \tag{5}$$

with $a_{\mathbf{kpq}}=q^2(p_xq_y-p_yq_x)\delta_{\mathbf{k}+\mathbf{p}+\mathbf{q},0}$. The Kronecker delta is a reminder that this is a sum over all possible vector triads in wave-number space. In what follows, it will be convenient to use a form for $J_{\mathbf{k}}$ that is symmetric with respect to $\mathbf{p}$ and $\mathbf{q}$, since they are dummy indices.[13] By interchanging $\mathbf{p}$ and $\mathbf{q}$ in (5) and adding to the original expression, we obtain the equivalent expression for $J_{\mathbf{k}}$,

$$J_{\mathbf{k}}=\sum_{\mathbf{pq}}b_{\mathbf{kpq}}\psi_{\mathbf{p}}^*\psi_{\mathbf{q}}^*, \tag{6}$$

where

$$b_{\mathbf{kqp}}\equiv\tfrac{1}{2}(a_{\mathbf{kpq}}+a_{\mathbf{kqp}})=\tfrac{1}{2}(q^2-p^2)(p_xq_y-p_yq_x)\delta_{\mathbf{k}+\mathbf{p}+\mathbf{q},0}. \tag{7}$$

In the time integration $J_{\mathbf{k}}$ is evaluated with full dealiasing using a staggered grid algorithm.[14] In the subsequent analysis, the terms in $J_{\mathbf{k}}$ are explicitly evaluated using (6) and (7). Time stepping is done using the leapfrog method with a weak Robert filter[15] applied every time step to suppress the computational mode and with the dissipation term lagged by one time step for numerical stability. The numerical experiments that we will describe have a maximum wave number up to $k_{\max}=256$, resulting in equivalent grid point resolution of up to 512^2. The dissipation function, $D_{\mathbf{k}}$, is modeled using a high-order "diffusion" (or scale selective filter) to dissipate the enstrophy that accumulates at the smallest resolved scales, and a linear drag to dispose of the energy that builds up at the largest scales:

$$D_{\mathbf{k}}\equiv-\alpha\zeta-\nu_nk^{2n}\zeta. \tag{8}$$

The high wave-number dissipation is a so-called "hyperviscosity" for which $n=8$ (see the Appendix). The forcing function $F_{\mathbf{k}}$ is modeled as a random Markovian process in time that is isotropic and band limited in wave-number space (e.g., $F_{\mathbf{k}}\neq0$ for $10\leqslant k\leqslant14$). For complete details concerning the forcing and dissipation, see Ref. 4.

Equation (4) can be used to derive an equation for the change in the energy of a single Fourier mode,

$$\frac{dE_{\mathbf{k}}}{dt}=T_{\mathbf{k}}+\Re(\psi_{\mathbf{k}}^*F_{\mathbf{k}})+\nu_nk^{2n}\psi_{\mathbf{k}}^2, \tag{9}$$

where $\Re$ means take the real part of the argument, $E_{\mathbf{k}}=\frac{1}{2}(k^2\psi_{\mathbf{k}}^2)$, $T_{\mathbf{k}}=\Sigma_{\mathbf{pq}}T_{\mathbf{kpq}}$, and

$$T_{\mathbf{kpq}}\equiv\Re(-b_{\mathbf{kpq}}\psi_{\mathbf{k}}\psi_{\mathbf{p}}\psi_{\mathbf{q}}). \tag{10}$$

Here $T_{\mathbf{kpq}}$ is the energy transfer rate into (if $T_{\mathbf{kpq}}$ is positive), or out of (if $T_{\mathbf{kpq}}$ is negative) mode $\mathbf{k}$ due to interactions with modes $\mathbf{p}$ and $\mathbf{q}=-\mathbf{k}-\mathbf{p}$. The enstrophy transfer $S_{\mathbf{kpq}}$, can be found in a similar manner and is related to $T_{\mathbf{kpq}}$ by

$$S_{\mathbf{kpq}}=k^2T_{\mathbf{kpq}} \tag{11}$$

(S and T will be referred to as transfer functions, regardless of the particular indices used).

The transfer functions defined above have certain symmetry and conservation properties, in particular

$$T_{\mathbf{kpq}}=T_{\mathbf{kqp}}, \tag{12}$$

since both describe the same vector triad. In addition, in any given triad there is detailed conservation of energy and enstrophy,

$$\begin{aligned}&T_{\mathbf{kpq}}+T_{\mathbf{pqk}}+T_{\mathbf{qkp}}=0,\\ &k^2T_{\mathbf{kpq}}+p^2T_{\mathbf{pqk}}+q^2T_{\mathbf{qkp}}=0.\end{aligned} \tag{13}$$

These constraints may be combined to find the following relations regarding the flow of energy:

$$T_{\mathbf{kpq}}/T_{\mathbf{qkp}}=(p^2-q^2)/(k^2-p^2),$$
$$T_{\mathbf{pqk}}/T_{\mathbf{kpq}}=(q^2-k^2)/(p^2-q^2), \tag{14}$$
$$T_{\mathbf{qkp}}/T_{\mathbf{pqk}}=(k^2-p^2)/(q^2-k^2),$$

which imply that only one of the transfer functions are linearly independent. That is, given one of the three, the other two are determined from (14). In addition, energy and enstrophy exchange within the triad is restricted to be directed into the wave numbers with largest and smallest magnitudes from the wave number with the middle magnitude, or into the middle wave number from the largest and smallest.

The function $T_{\mathbf{k}}$ reveals only the total transfer rate into $\mathbf{k}$ due to all triad interactions. To examine the role of nonlocality, it is necessary to use the more detailed information given by $T_{\mathbf{kpq}}$. However, visualization of $T_{\mathbf{kpq}}$ is difficult because it has three vector indices, so we will begin with a function that is more detailed than $T_{\mathbf{k}}$, yet is simpler than $T_{\mathbf{kpq}}$.

We reduce the number of indices by summing over $\mathbf{q}$,

$$T_{\mathbf{kp}}\equiv\sum_{\mathbf{q}} T_{\mathbf{kpq}}. \tag{15}$$

(This is actually a trivial sum, since for any given $\mathbf{k}$ and $\mathbf{p}$, there is only one possible $\mathbf{q}$.) If the turbulence is isotropic, functions may be averaged over angles in wave-number space, which further decreases the complexity. In this case, we define

$$T_{kp}\equiv\int k\,d\theta_{\mathbf{k}}\int p\,d\theta_{\mathbf{p}}\,T_{\mathbf{kp}} \tag{16}$$

as the transfer to all wave numbers of magnitude k due to interactions with all wave numbers of magnitude p. Following (11), note that $S_{kp}=k^2T_{kp}$. In practice, transfer functions will also be averaged in time, for smoother results.

III. ENSTROPHY INERTIAL RANGE TRANSFER

In order to obtain an inertial range that is as long as possible given the constraints of the numerical resolution, forcing is applied at relatively low wave numbers. The following discussion will refer to a simulation forced in the range $10\leqslant k\leqslant 14$ with low wave-number drag extending up to $k=5$. The vorticity field (as well as other flow diagnostics) demonstrates the existence of many long-lived coherent vortices with a typical diameter given by the forcing scale [see Fig. 1(a) of Ref. 4]. There is a constant flux enstrophy inertial range between the forcing and dissipation ranges [Fig. 1(a)] that is characterized by two distinct slopes in the energy spectrum [Fig. 1(b)]. The steeper, lower wave-number part is related to the presence of the vortices,[3,4] while the higher wave-number subrange has a slope close to k^{-3} and is associated with a more "classical" turbulent cascade occurring between the vortices.

Figure 2(a) shows the enstrophy transfer function S_{kp} for $k=70$ in the enstrophy inertial range. From the definition of the transfer function (9) and (10), a negative

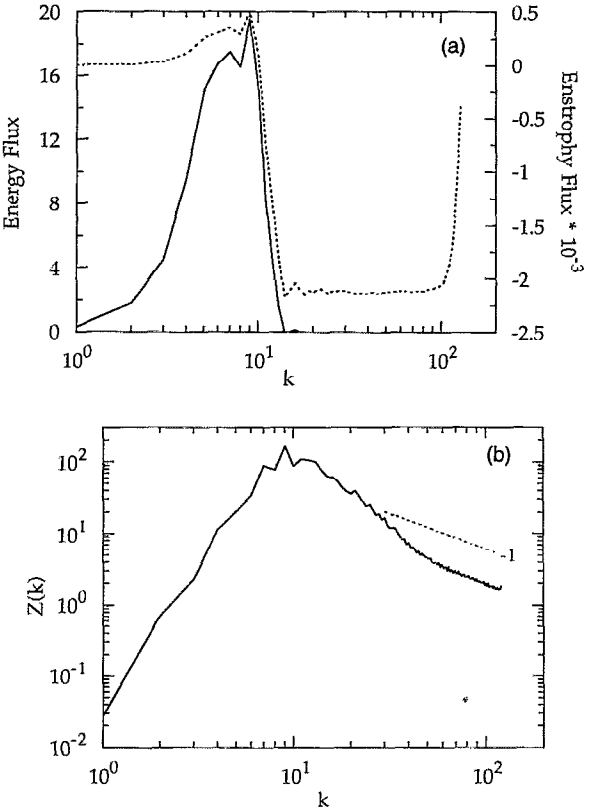

FIG. 1. (a) The time-averaged energy flux (solid curve) and enstrophy flux (dashed curve) from a simulation forced in the range $10\leqslant k\leqslant 14$. (b) The time-averaged enstrophy spectrum $Z(k)=k^2E(k)$. Note the transition around $k=45$ from a relatively steep spectrum to approximately k^{-1}.

value of S_{kp} means that wave number k is losing enstrophy to wave number p, and a positive value the reverse. Thus, it is clear that enstrophy is being transferred from large to small scale in the enstrophy inertial range. Figure 2(a) also indicates that the transfer is quite local in p space. With the exception of the signal that appears at small p (which will be discussed later), nearly all of the transfer into k comes from interactions with p that are within about ten wave numbers on either side of k. Figure 2(b) shows S_{kp} for $k=50$, 70, and 90 (all in the inertial range); the shape of S_{kp} remains similar for all k in the enstrophy inertial range. The amplitude appears to decrease slightly with k, though fluctuations are probably too large to determine any systematic change. The area under each of these curves is approximately zero, meaning that there is no *net* transfer into any k, reflecting the presence of a statistically steady-state inertial range.

Although the shape and amplitude of S_{kp} are essentially independent of k, this does not of itself imply constant enstrophy flux through the inertial range. The enstrophy flux past k' is defined as

$$\Pi^Z_{k'}=\sum_{k=k'}^{k_{\max}}\sum_{p=1}^{k_{\max}} S_{kp}=-\sum_{k=1}^{k'}\sum_{p=1}^{k_{\max}} S_{kp}, \tag{17}$$

so we may still have constant (or zero) inertial range flux as long as $\Sigma_p S_{kp}$ is zero for all $k'\leqslant k\leqslant k_d$, where k_d is a wave number at the beginning of the dissipation range. In

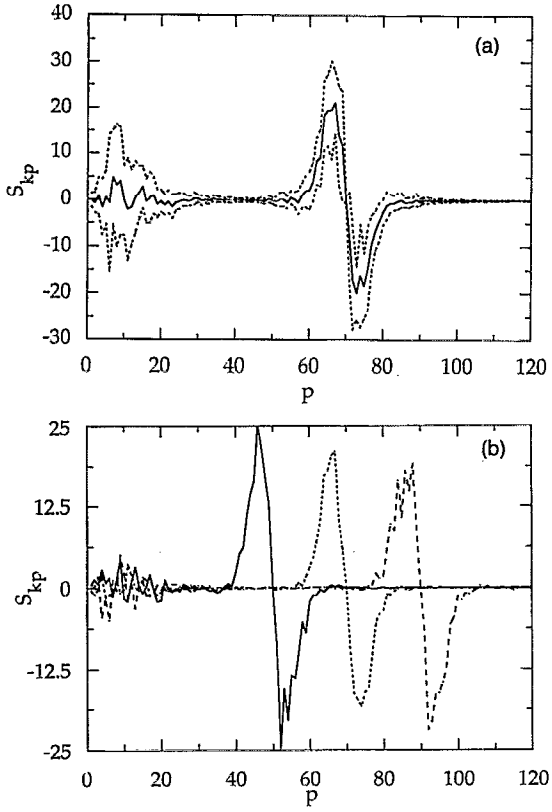

FIG. 2. Time-averaged enstrophy transfer functions. (a) The enstrophy transfer function S_{kp} for the inertial range wave number $k=70$. The dashed lines represent one standard deviation from the mean based on 20 samples. (b) S_{kp} for the inertial range wave numbers $k=50$ (solid curve), $k=70$ (short dashed curve), and $k=90$ (long dashed curve).

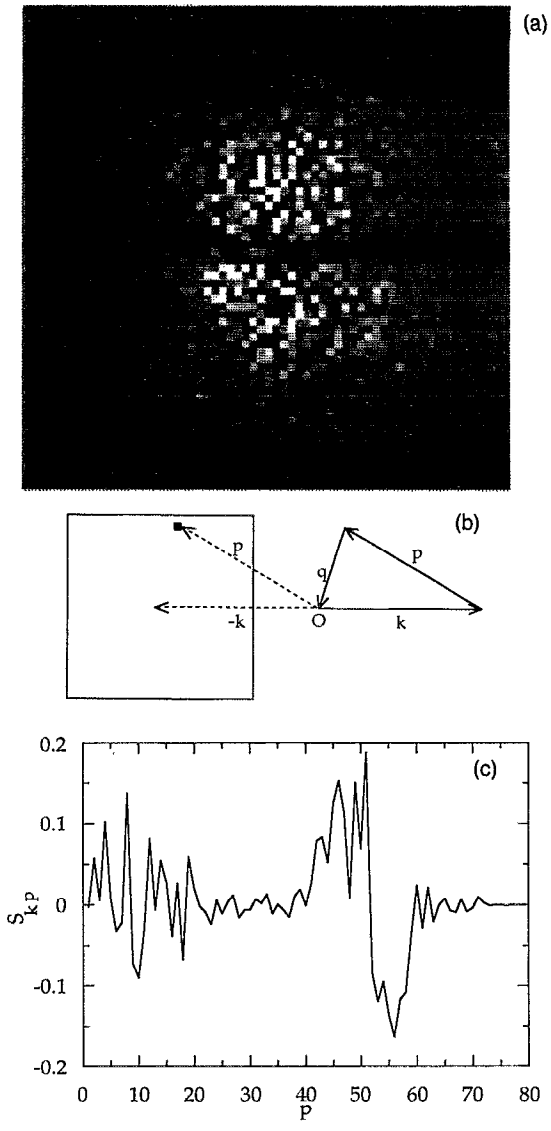

FIG. 3. (a) The time-averaged enstrophy transfer function $S_{\mathbf{kp}}$ for $\mathbf{k}=(50,0)$. Areas blacker than the background gray have positive values of $S_{\mathbf{kp}}$, with solid black denoting the highest value; similarly, white denotes negative values. The plot is centered (in $\mathbf{p}$ space) at $\mathbf{p}=-\mathbf{k}$. (b) Schematic for interpreting (a). Given the triangle made of solid vectors ($\mathbf{k}+\mathbf{p}+\mathbf{q}=0$), the dashed vectors represent their orientation in the plot of $S_{\mathbf{kp}}$. The square outline denotes the border of (a) above and "O" is the origin $(p_x,p_y)=(0,0)$. The small black square at the end of the dashed $\mathbf{p}$ vector represents an $S_{\mathbf{kp}}$ grid point. (c) $S_{\mathbf{kp}}$ from a averaged over angle in $\mathbf{p}$ space.

a statistically steady-state inertial range (where $\dot{E}_k=\dot{F}_k=\dot{D}_k=0$ by definition, and the dot denotes time rate of change) the condition that $S_k=0$ is satisfied, so any contributions to the flux integral (17) must come from k in the dissipation range where the balance is $S_k+k^2\dot{D}_k=0$. This balance is independent of both the amplitude and general shape of S_{kp}, but is dependent on the area under each transfer curve. This point will be especially important when considering energy transfer.

The energy transfer function amplitude decreases approximately as k^{-2} since $S_{kp}=k^2T_{kp}$ and S_{kp} is approximately independent of k. Since T_{kp} is proportional to S_{kp}, energy is transferred from large scale to small scale in apparent contradiction with inertial range theory. However, inertial range theory predicts zero energy *flux* through the enstrophy inertial range. In fact, a decreasing amplitude for T_{kp} does not imply nonconstant (or nonzero) flux since, still, the area under each T_{kp} curve is zero. Indeed, it is such a falloff in the amplitude T_{kp} that results in the asymptotically small (yet constant) flux of energy to small scales by making contributions to the flux integral in the dissipation range negligibly small. This is consistent with theories that predict no energy dissipation in the limit of infinite Reynolds number.

To obtain vector information about triad interactions, $S_{\mathbf{kp}}$ can be displayed as a map in $\mathbf{p}$ space with shading related to the transfer rate, as in Fig. 3(a). The largest magnitudes of the transfer function are clustered around $\mathbf{p}=-\mathbf{k}$. Figure 3(b) shows a schematic of typical triad shapes that result in this interaction. Thus we can see that while S_{kp} informed us that the magnitude of $\mathbf{p}$ is close to the magnitude of $\mathbf{k}$ for the strongest interactions, $S_{\mathbf{kp}}$ shows that the important triads are very elongated triangles, with $k\approx p\gg q$ in the inertial range. (This result has also been seen in EDQNM calculations,[16] and in a numerical simulation.[9]) It can also be seen that the transfer function is very irregular, going from positive to negative at adjacent $\mathbf{p}$ grid points. Thus there are interactions in which

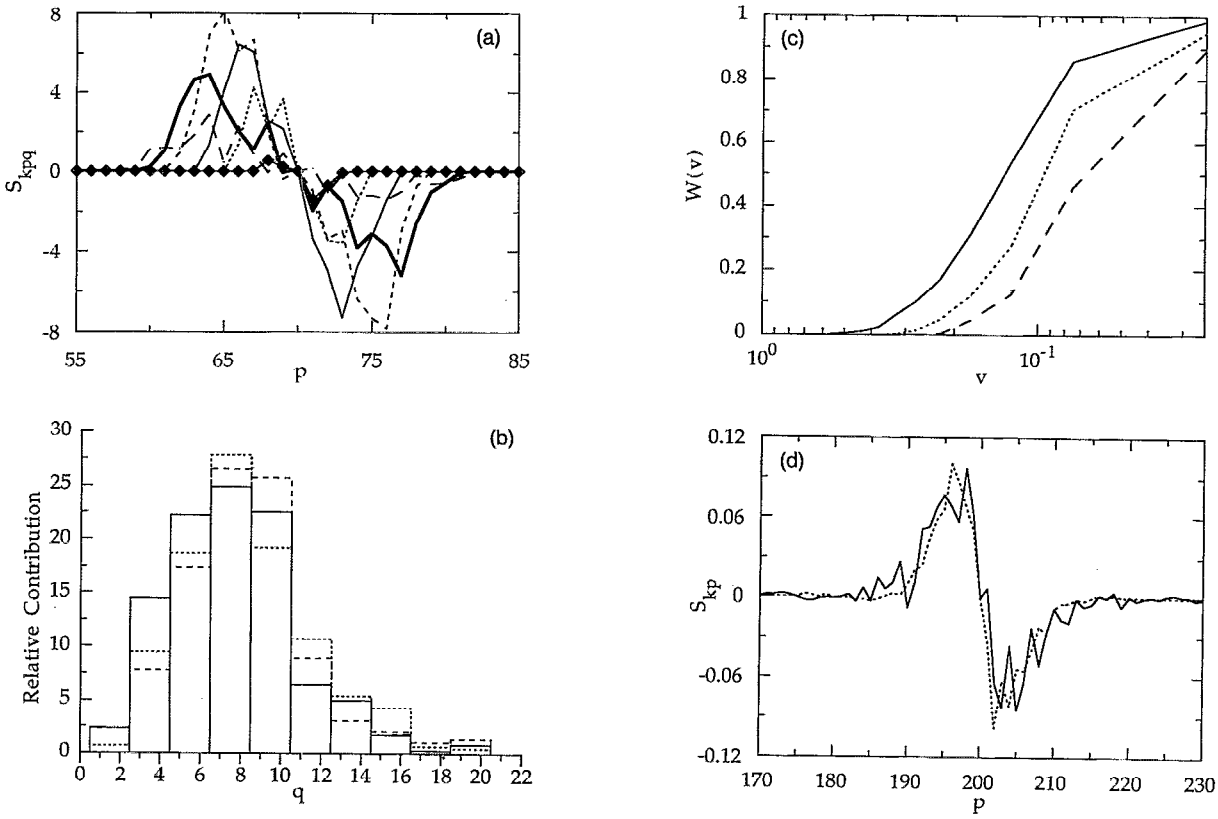

FIG. 4. (a) The time-averaged enstrophy transfer function S_{kpq} for $k=70$. Each successive curve is the contribution from $(2n+1/2)<q<(2n+2+1/2)$, for $n=0, 1, 2,...,5$. The curve marked with diamonds corresponds to $n=0$ ($\frac{1}{2}<q<2\frac{1}{2}$), the short dashed curve to $n=1$, the thin solid curve to $n=2$, the medium dashed curve to $n=3$, the thick solid curve to $n=4$, and the long dashed curve to $n=5$. (b) Histogram of the relative area under each curve in a above for $p<k$. The first bin is for the $n=0$ curve, the second for the $n=1$ curve, etc. The solid lines are for $k=50$, the short dashed lines for $k=70$, and the long dashed lines for $k=90$. (c) The locality function $W(v)$ for $k=50$ (solid curve), $k=70$ (short dashed curve), and $k=90$ (long dashed curve). (d) S_{kp} for $k=50$ [dashed curve; same as in Fig. 2(a)] and S_{kp} for $k=200$ (solid curve) from a higher resolution run. The dashed curve has been shifted over to $k=200$ and scaled in amplitude for comparison.

energy is going from the middle wave number into the largest and smallest, and others transferring into the middle wave number. Performing an average over **p** space for this vector **k** ($S_{\mathbf{kp}}$), we see that energy is typically transferred *out of* the middle wave number [Fig. 3(c)], just as in Fig. 2(a).

Since the data is very irregular when looking at $S_{\mathbf{kp}}$, we average over angles in **k** space without losing all information about **q**. Following Domaradzki[17] we now define S_{kpq} as the transfer to all wave numbers of magnitude k due to interactions with all wave numbers of magnitude p such that the third leg of the triad has magnitude q. Here S_{kpq} is similar to S_{kp} (in fact, $S_{kp}=\Sigma_q S_{kpq}$) except now there will be a separate curve for every value of q. In practice, q is defined as a band of wave numbers, say, for example, between 2.5 and 4.5. Again [Fig. 4(a)] major contributions to the total energy transfer comes from $k\approx p\gg q$. This is what we will refer to as predominantly *nonlocal* triad interactions. Note that the p dependence in the vicinity of k reflects the same approximate structure as S_{kp} for all q bands, with the peak moving slowly away from $p=k$ as q gets larger.

A more quantitative measure of the contributions from different values of q can be seen in Fig. 4(b). As the net transfer (or total area under all of the curves) into k is zero in a statistically steady state, we consider only the range $p<k$ where S_{kpq} is positive when comparing the area under each curve. (The same results are obtained using $p>k$.) Most of the transfer comes from interactions with $q<12$, with the peak around $q=8$, which is in fact the location of the peak in the energy spectrum. Note that this simulation is forced for $10\leqslant k\leqslant 14$, so the direct influence of q in the forcing range is not particularly important.

Another useful way of quantitatively presenting the nature of the transfer is to consider the contributions based on the geometry of a triad, as was done by Kraichnan[7] using an analytical closure model. For a given k, the geometry of a triad can be partially expressed as the ratio of the length of the smallest side to the length of the middle side. A locality function $W(v)$ is then defined as the fraction of the total transfer due to all triads for which the ratio of the smallest to the middle wave number is greater than v. Figure 4(c) shows that the dominant triads are very elongated since only 10% of the total transfer comes from triad interactions in which the ratio of the smallest to the middle wave number is greater than 0.30 for $k=50$, and greater than 0.15 for $k=90$. The inertial range is not self-similar in the sense that the *shape* of the important enstrophy transferring triads changes with wave number. For example, if a given triad is found to be dominant for $k=k_1$,

then self-similarity would imply that a similar shaped triad would be equally dominant for $k=k_2>k_1$, the ratio p/q would be constant and all curves in Fig. 4(c) would be coincident. This is clearly not the case in the simulations reported here.

Further evidence that the transfer is not self-similar in this sense can be seen in Fig. 4(d) which shows S_{kp} for $k=200$ from a higher resolution run ($k_{max}=256$) superimposed on S_{kp} for $k=50$ from the lower resolution run. Their shapes are a remarkable match. (No scaling of the horizontal axis is performed.) If the transfer in the inertial range were self-similar, one would expect the curves to match on a logarithmic scale, instead of a linear scale as shown. The evidence in Fig. 4 seems to indicate that one could perform a very high resolution simulation, and find that the transfer into, say, $k=1000$ would still be dominated by contributions from q in the vicinity of the spectral peak and the shape of S_{kp} would still be the same as for $k=50$.

An explanation of the signal at small values of p in S_{kp} (Fig. 2) is now possible. It is the contribution from curves with $k\approx q\gg p$, reflecting the fact that we have a symmetric transfer function $S_{\mathbf{kpq}}=S_{\mathbf{kqp}}$. In fact, the behavior of S_{kp} at small p gives an indication of whether the system is in a statistically steady state. Now, a steady state is defined by $S_k=\Sigma_{pq}S_{kpq}=0$ (time averaged). This sum can be written as $\Sigma_{q\ll k}\Sigma_{p\approx k}+\Sigma_{p\ll k}\Sigma_{q\approx k}$ since the triad interactions are so nonlocal. Thus if the fluctuations in S_{kp} for small p sum up to be much smaller than the peak value for $p\approx k$, the system should be in steady state. This is clearly the case in Fig. 2(a).

Although the enstrophy transfer in the inertial range is accomplished through interactions that involve very nonlocal triads, this does not necessarily mean that the actual transfer is nonlocal. The locality of the transfer can be determined by examining the transfer balance among the members of a given triad. Figure 5(a) shows time series of $S_{\mathbf{kpq}}$, $S_{\mathbf{pqk}}$, and $S_{\mathbf{qkp}}$ for a particular, relatively important, triad involved in the inertial range transfer. The enstrophy transfer is primarily between the two wave numbers in the inertial range since $S_{\mathbf{kpq}}\approx -S_{\mathbf{pqk}}$. This is not surprising since [using (14)] $S_{\mathbf{kpq}}=[p^2(p^2-q^2)/k^2(q^2-k^2)]S_{\mathbf{pqk}}\approx(-p^4/k^4)S_{\mathbf{pqk}}$ for k, $p\gg q$. This is an example of *local* enstrophy transfer since the exchange is primarily between the triad members of similar length and orientation. It would seem that the small wave number acts as a mediator, or catalyst, but does not lose or gain significant enstrophy in this particular interaction. Physically, this is consistent with the idea that large-scale straining of vortex sheets is the mechanism for the enstrophy cascade. The transfer is very intermittent in time and the statistics are not Gaussian, as can be seen in the probability distribution function (pdf) constructed from the time series of $S_{\mathbf{kpq}}$ [Fig. 5(b)].

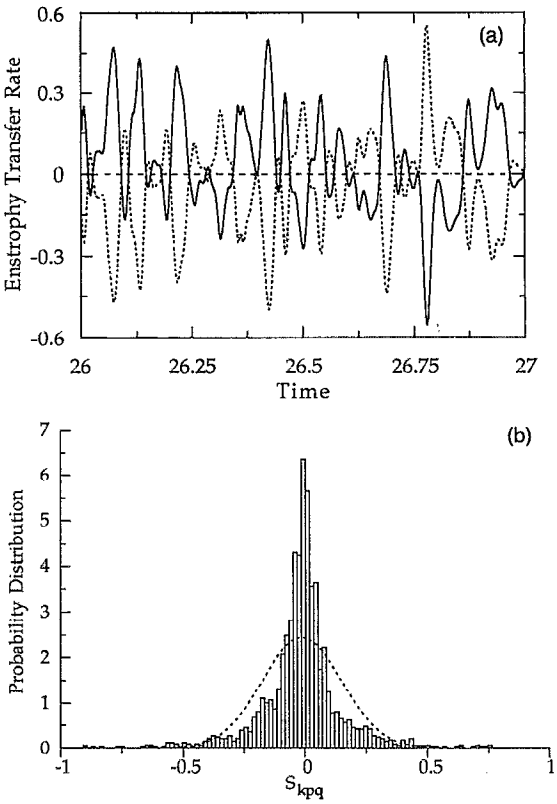

FIG. 5. (a) Time series of $S_{\mathbf{kpq}}$ (solid curve), $S_{\mathbf{pqk}}$ (short dashed curve), and $S_{\mathbf{qkp}}$ (long dashed curve) for $\mathbf{k}=(50,0)$, $\mathbf{p}=(-52,5)$, and $\mathbf{q}=(2,-5)$. (b) Probability distribution function constructed from the time series [four times longer than shown in (a)] of $S_{\mathbf{kpq}}$. The overlaying curve is a Gaussian with the same mean and standard deviation as the constructed pdf.

IV. ENERGY INERTIAL RANGE TRANSFER

In order to maximize the resolution of the energy inertial range, forcing in this instance is applied at relatively high wave number while still allowing for a short enstrophy inertial range at even higher wave numbers. Again, coherent structures are found at approximately the forcing scale [see Fig. 1(e) of Ref. 4]. The following discussion will refer to a 256^2 simulation forced in the range $80\leqslant k\leqslant 84$ with low wave-number drag acting for $k<5$. A constant flux energy inertial range forms with an energy spectrum close to $k^{-5/3}$ (Fig. 6).

Figure 7(a) shows the energy transfer function T_{kp} for k in the energy inertial range. The data are more irregular than for the enstrophy inertial range, but do have a similar form. Again, it shows that in the inertial range energy (and enstrophy) is being transferred toward high wave numbers due to interactions with p near k in the inertial range. We know that the *flux* of energy is toward small k [Fig. 6(a)], so this result may seem paradoxical. However, the flux past k is not directly related to the transfer at k; rather it is an integral quantity as in (17). The form of the energy transfer function does indicate that the mechanisms similar to those responsible for transfer in the enstrophy inertial range (namely, straining of vortex sheets) are also acting in the energy inertial range. One important difference found here, however, is the small but positive values of T_{kp} found at large p, that is, for p in the enstrophy inertial range above the forcing range (i.e., above $k=84$). These interactions do transfer energy to larger scales. Furthermore, the transfer functions for k in the low wave-number drag range and in the high wave-number forcing range

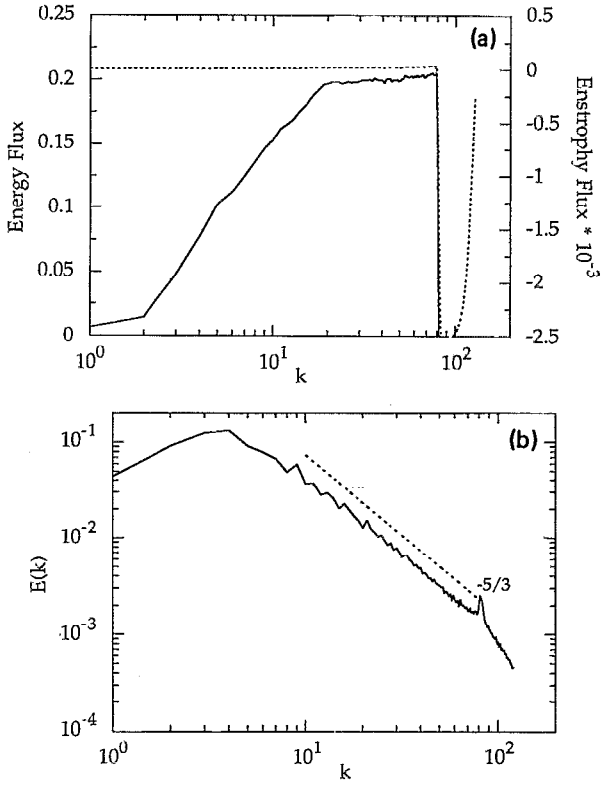

FIG. 6. (a) The time-averaged energy flux (solid curve) and enstrophy flux (dashed curve) from a simulation forced in the range $80 \leq k \leq 84$. (b) The time-averaged energy spectrum, $E(k)$.

[Figs. 7(b) and 7(c), respectively] also show that there is a direct and rather nonlocal transfer of energy from the forcing scale to low wave numbers. Note that the transfer into $k=5$ is directed from small to large scale (i.e., opposite to the direction of transfer for k in the inertial range) and is dominated by interactions of large-scale components.

As with T_{kp}, the q-dependent transfer functions [Fig. 7(d)] are quite noisy, but the trend of transfer to high wave numbers for $p \sim k$ is in evidence. The distribution of $T_{\mathbf{kp}}$ [Fig. 8(a)] shows more clearly that a larger variety of triads are involved with the transfer in the vicinity of $\mathbf{k}$ than is the case with low wave-number forcing [see Fig. 3(a)]. A histogram of the relative contribution from each q [Fig. 8(b)] reveals that, just as in the enstrophy inertial range, the transfer peak is in the vicinity of the spectral peak, but the distribution falls off more slowly with increasing q (since the spectrum falls off more slowly), again indicating that a wider range of triads are playing a role in energy inertial range transfer. Note also the presence of a second peak in the distribution showing significant contributions from large q that are completely absent in the enstrophy inertial range. It is these values of q that combine with large values of p to form triads that transfer energy to larger scales. These triads (where k is the smallest member) will turn out to be important when considering the energy inertial range flux. Quantitatively, the triads that contribute to the transfer are more local than in the en-

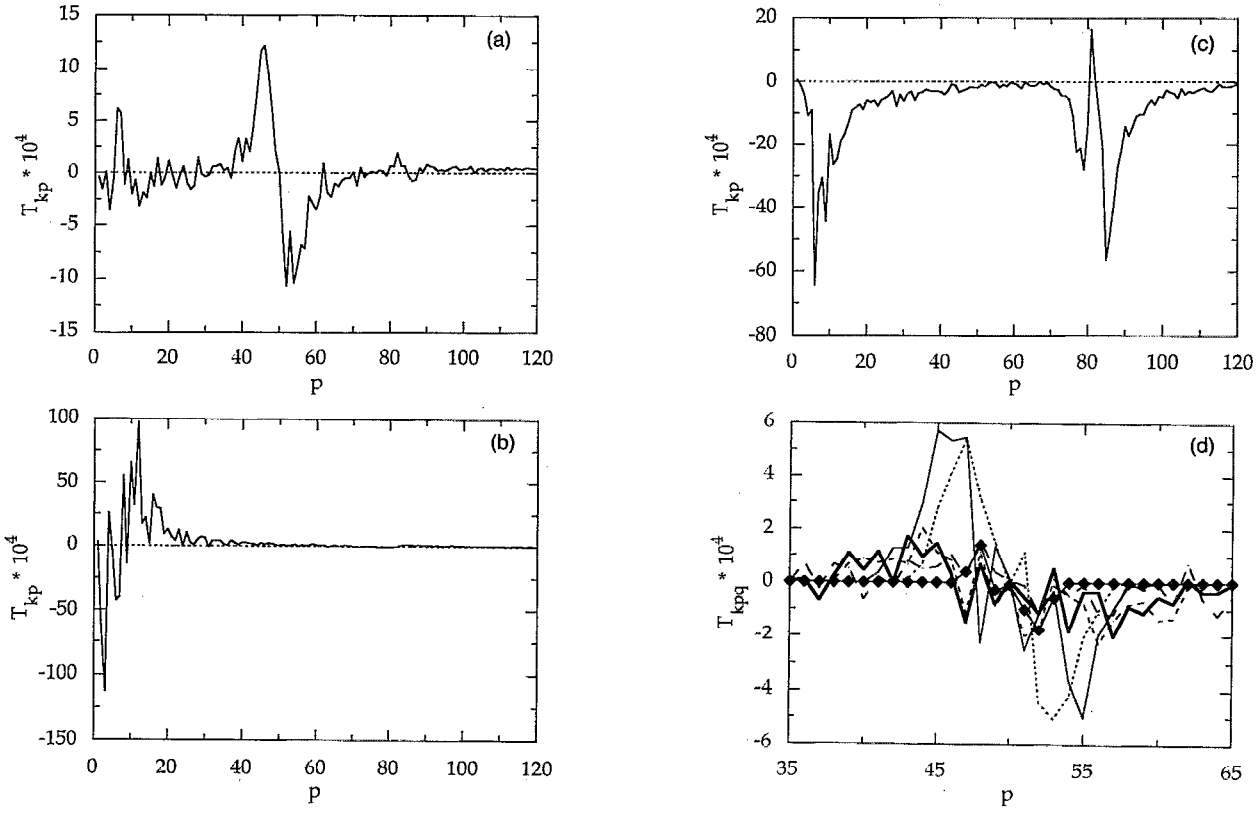

FIG. 7. Time-averaged energy transfer functions from a simulation forced in the range $80 \leq k \leq 84$. (a) T_{kp} for the inertial range wave number $k=50$. The short dashed line is a zero reference. The standard deviation based on 50 samples is of the order of the mean. (b) T_{kp} for the drag range wave number $k=5$. (c) T_{kp} for the forcing range wave number $k=82$. (d) T_{kpq} for $k=50$. Each successive curve is the contribution from $(3n+1/2) \leq q \leq (3n+3+1/2)$, for $n=0, 1, 2, \ldots, 5$, and the sequence of curve types is the same as in Fig. 4(a).

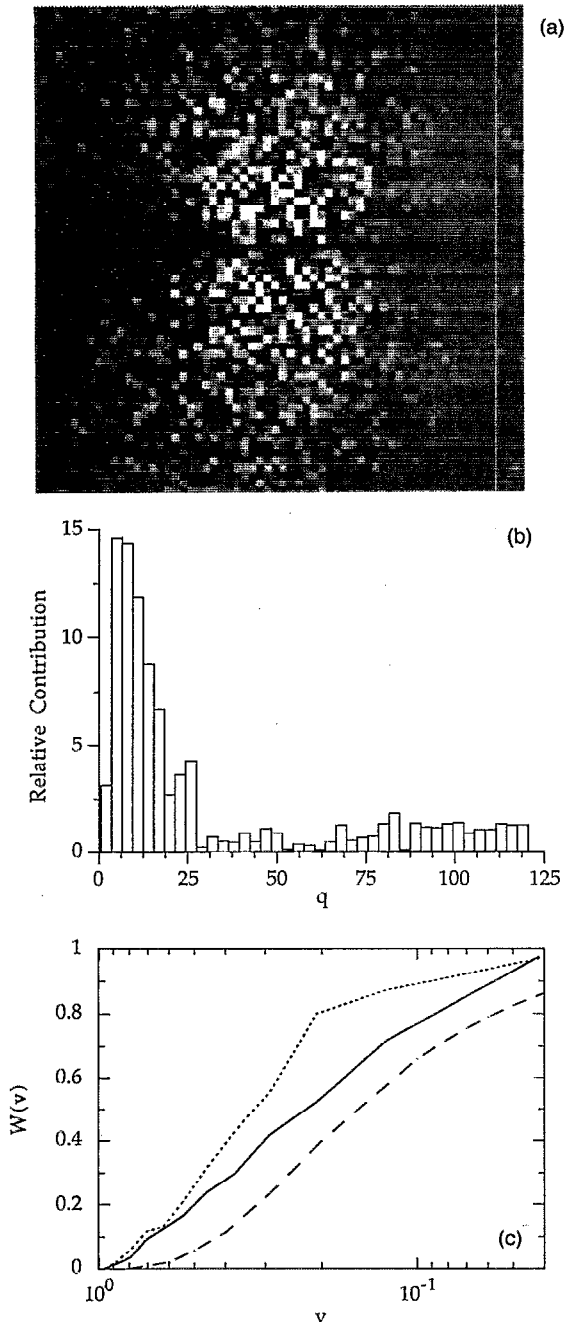

FIG. 8. (a) T_{kp} for k=(50,0). See Fig. 3 for interpretation. (b) Histogram of the relative area under each curve in Fig. 7(d) above [as well as for some not shown in Fig. 7(d)] for $p>k$ and $k=50$. (c) The locality function $W(v)$ for $k=50$ (solid curve) and $k=30$ (short dashed curve). For comparison, the long dashed curve is $W(v)$ seen in Fig. 2 of Ref. 7 for an infinite inertial range predicted by an analytical closure.

strophy inertial range in the sense that contributions to the total transfer are significant even as the ratio of the smallest to the middle wave number approaches unity [Fig. 8(c)]. Here, approximately 40% of the transfer for $k=50$ comes from triad interactions in which the ratio of the smallest to the middle wave number is greater than 0.3, in contrast to 10% for $k=50$ in the enstrophy inertial range [see Fig. 4(c)]. The transfer is perhaps more self-similar here than in the enstrophy inertial range (especially as $v\to 1$), implying that it is the shape of the triad that determines, at least in part, its importance.

V. COMPARISON WITH ANALYTICAL CLOSURE

We now compare the results from the simulations with those predicted by analytical theories of turbulence, in particular with the eddy-damped quasinormal Markovian closure (EDQNM).[18,19] Typically, the equation for the energy spectrum in EDQNM is presented after one makes the assumption that the turbulence is isotropic (e.g., Ref. 8). However, for our purposes it is useful to formulate the closure in vector wave-number space, without the assumption of isotropy, for then identical analyses of transfer functions can be performed for closure and simulation. It is also convenient to express the equation for the modal energies in terms of the streamfunction as follows:

$$\frac{d}{dt}E(\mathbf{k})=\int\int d\mathbf{p}\,d\mathbf{q}\,T(\mathbf{k},\mathbf{p},\mathbf{q}), \tag{18}$$

where

$$T(\mathbf{k},\mathbf{p},\mathbf{q})\equiv k^2 B(\mathbf{k},\mathbf{p},\mathbf{q})\theta(\mathbf{k},\mathbf{p},\mathbf{q})R(\mathbf{k},\mathbf{p},\mathbf{q}), \tag{19}$$

with

$$\begin{aligned}R(\mathbf{k},\mathbf{p},\mathbf{q})\equiv{}& B(\mathbf{k},\mathbf{p},\mathbf{q})\psi^2(\mathbf{p})\psi^2(\mathbf{q})\\ &+B(\mathbf{p},\mathbf{q},\mathbf{k})\psi^2(\mathbf{q})\psi^2(\mathbf{k})\\ &+B(\mathbf{q},\mathbf{k},\mathbf{p})\psi^2(\mathbf{k})\psi^2(\mathbf{p}),\end{aligned} \tag{20}$$

$$B(\mathbf{k},\mathbf{p},\mathbf{q})\equiv\frac{1}{2k^2}(q^2-p^2)(p_xq_y-p_yq_x)\delta_{\mathbf{k}+\mathbf{p}+\mathbf{q},0}, \tag{21}$$

and

$$\theta(\mathbf{k},\mathbf{p},\mathbf{q})\equiv\frac{1-\exp[-\mu(\mathbf{k},\mathbf{p},\mathbf{q})t]}{\mu(\mathbf{k},\mathbf{p},\mathbf{q})}, \tag{22}$$

where $\mu(\mathbf{k},\mathbf{p},\mathbf{q})\equiv\mu(\mathbf{k})+\mu(\mathbf{p})+\mu(\mathbf{q})$ is the eddy-damping rate for triple correlations. Two possible expressions for $\mu(\mathbf{k})$ (neglecting viscous contributions) are the local turnover rate

$$\mu_l(\mathbf{k})=\gamma_l[k^4E(\mathbf{k})]^{1/2} \tag{23}$$

or the nonlocal strain rate

$$\mu_n(\mathbf{k})=\gamma_n\left(\int_1^{|\mathbf{k}|}p^2E(p)dp\right)^{1/2}. \tag{24}$$

We will be concerned with steady-state inertial ranges for which $\mu(\mathbf{k},\mathbf{p},\mathbf{q})t$ is very large so that $\theta(\mathbf{k},\mathbf{p},\mathbf{q})=\mu(\mathbf{k},\mathbf{p},\mathbf{q})^{-1}$.

Rather than integrating the closure in time, as for example in Ref. 16 and (using the test field model closure) in Ref. 20, we will use the closure to analyze the results of the simulation. This is done by substituting the values for the modal energies calculated in direct simulations into the expression for $T(\mathbf{k},\mathbf{p},\mathbf{q})$ and comparing the result with the transfer functions calculated by the simulations (e.g., T_{kpq}[21]). This focuses attention on the structure of the closure, rather than on poorly determined phenomenological coefficients which differ from closure to closure. Of

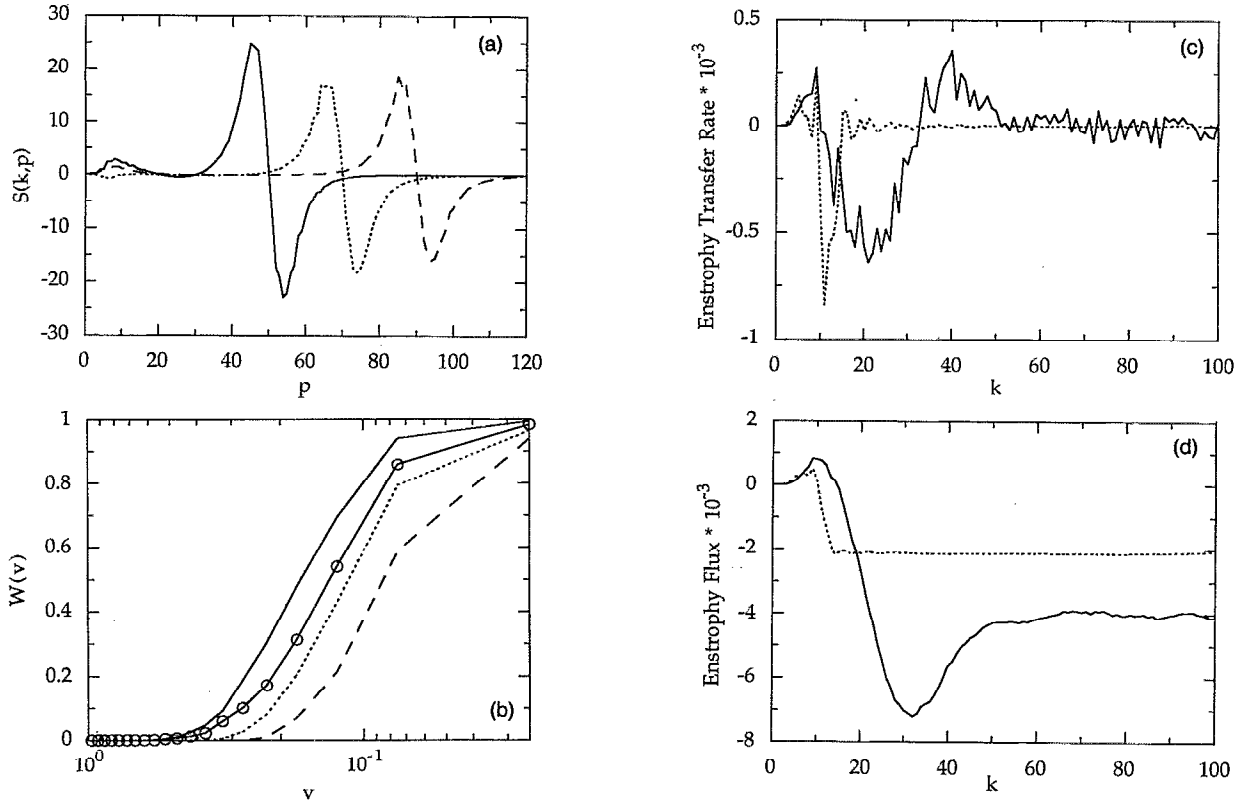

FIG. 9. Enstrophy transfer functions as calculated by EDQNM using the local time scale (23) with $\gamma_l=0.6$ and the time-averaged energy spectrum from the run described in Figs. 1–5. (a) $S(k,p)$ for $k=50$ (solid curve), $k=70$ (short dashed curve), and $k=90$ (long dashed curve). (b) The locality function $W(v)$ for $k=50$ (solid curve), $k=70$ (short dashed curve), and $k=90$ (long dashed curve). For comparison, the curve marked with circles is $W(v)$ for $k=50$ calculated by the full simulation [i.e., the solid curve from Fig. 4(c)]. (c) The total enstrophy transfer rates $S(k)$ from EDQNM (solid curve) and S_k from the simulation (dashed curve). (d) The enstrophy flux from EDQNM (solid curve) and from the simulation (dashed curve). A value of $\gamma_l=1.1$ is needed to make the EDQNM flux approximately agree with the simulation for $50<k<100$.

course, the validity of EDQNM may in part be determined by the resemblance of its transfer functions to those calculated in the direct simulations.

The qualitative agreement between $S(k,p)$ and S_{kp} in the enstrophy inertial range is quite good [Fig. 9(a)] in the vicinity of $p=k$. The shape of $S(k,p)$ depends only very weakly on whether a local description for $\mu(\mathbf{k},\mathbf{p},\mathbf{q})$ (23) or a nonlocal one (24) is chosen; only the value of the constant γ differs. For this case, we find $\gamma_l\approx 0.6$ and $\gamma_n\approx 0.15$ give good agreement for the amplitudes of $S(k,p)$ with the S_{kp} curves in Fig. 2(b). The behavior of $S(k,p,q)$ (not shown) indicates that the important triads are very elongated, though the distribution with q is peaked at slightly higher wave number ($q\approx 10$) and is more broad than for S_{kpq}. This is reflected in Fig. 9(b), where it is seen that 20% of the total transfer comes from triad interactions with a small to middle wave-number ratio of 0.30 for $k=50$, as opposed to 10% for such triads in the direct simulation. However, this percentage does decrease with increasing k, a trend that agrees with the simulations.

The presence of a positive signal for small p in $S(k,p)$ in Fig. 9(a) indicates that the system is not in a statistically steady state as far as the closure is concerned. Given this spectrum as an initial condition, the closure would begin to evolve the system in such a way as to rapidly shallow the spectrum for $15<k<30$ (which is initially much steeper than k^{-3}) while leaving the range $k>50$ (which is initially close to k^{-3}) essentially unchanged [Fig. 9(c)]. The large discrepancy in $S(k)$ compared to S_k at the lower end of the inertial range results in large error when computing the flux[22] [Fig. 9(d)].

Results from comparisons in the energy inertial range are similar to those in the enstrophy inertial range. We find the same characteristic shape for $T(k,p)$ [Fig. 10(a)] for p in the vicinity of k (i.e., transfer from large to small scales) as well as the contribution from p above the forcing range. Use of the local $\mu(\mathbf{k},\mathbf{p},\mathbf{q})$ again produces essentially identical results as the nonlocal expression, with $\gamma_l\approx 0.15$ and $\gamma_n\approx 0.08$ producing best agreement with the amplitudes for T_{kp}. Note that different values of γ are needed in the energy and enstrophy inertial ranges, in agreement with Ref. 16 where it was found that it is not possible to recover the values of the inertial range constants as predicted in Ref. 7 without using a different value of γ_n for each inertial range separately. The distribution of $T(k,p,q)$ (not shown) with q is similar to that for T_{kpq} [see Fig. 8(b)] and is peaked at slightly higher wave number. In contrast to the comparison in the enstrophy inertial range, the EDQNM triad interactions appear to be less local than the simulations since only 20% of the total transfer into $k=50$ comes from triads in which the ratio of the smallest to the middle wave number is greater than 0.3 for EDQNM, compared to 40%

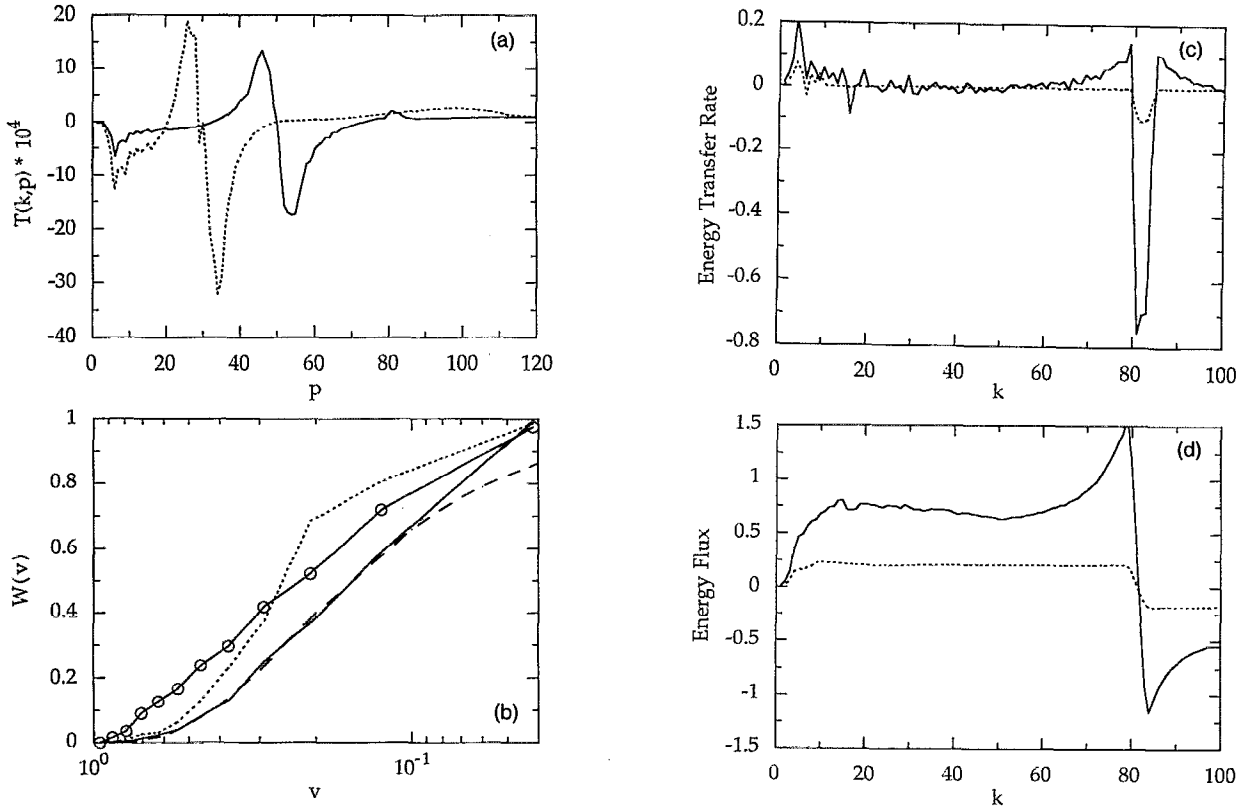

FIG. 10. Energy transfer functions as calculated by EDQNM using the local time scale (23) with $\gamma_l=0.15$ and the time-averaged energy spectrum from the run described in Figs. 6–8. (a) $T(k,p)$ for $k=50$ (solid curve) and $k=30$ (dashed curve). (b) The locality function $W(v)$ for $k=50$ (solid curve) and $k=30$ (dashed curve). For comparison, the curve marked with circles is from the simulation [seen in Fig. 8(c)] for $k=50$, and the long dashed line is $W(v)$ seen in Fig. 2 of Ref. 7 for an infinite inertial range predicted by an analytical closure. (c) The total energy transfer rates $T(k)$ from EDQNM (solid curve) and T_k from the simulation (dashed curve). (d) The energy flux from EDQNM (solid curve) and from the simulation (dashed curve). A value of $\gamma_l=0.5$ is needed to make the EDQNM flux approximately agree with the simulation for $10<k<60$.

for the direct simulation [Fig. 10(b)]. However, EDQNM does recover the same kind of self-similarity as the simulations as $v\to 1$, and displays the same trends with increasing k. Note that the EDQNM curve for $k=50$ is almost identical to Kraichnan's[7] result, implying conditions similar to an infinite self-similar inertial range. Given this initial condition, the closure would not significantly alter the slope of the energy inertial range spectrum that is approximately proportional to $k^{-5/3}$ [Fig. 10(c)]; only the region near the forcing range would change. Again there is a large error in calculating the energy flux [Fig. 10(d)].

VI. INERTIAL RANGE FLUX

In this section we discuss the relationship of inertial range flux to transfer, and resolve the apparent dichotomy of downscale energy transfer in the energy inertial range accompanied with upscale energy flux by examining the inertial range fluxes in more detail.

It can be shown[7] that the flux integral (17) can be rewritten as $\Pi^Z_{k'}=\Pi^{Z+}_{k'}+\Pi^{Z-}_{k'}$, where

$$\Pi^{Z+}_{k'}\equiv\sum_{k=k'}^{\infty}\Pi^{Z+}_{k'k};\quad \Pi^{Z-}_{k'}\equiv\sum_{k=0}^{k'}\Pi^{Z-}_{k'k} \tag{25}$$

and

$$\Pi^{Z+}_{k'k}\equiv\sum_{p,q=0}^{k'}S_{kpq};\quad \Pi^{Z-}_{k'k}\equiv-\sum_{p,q=k'}^{\infty}S_{kpq}. \tag{26}$$

Similar expressions exist for the energy flux, $\Pi^E_{k'}$. Thus the flux past k' has contributions from triads with $k<k'<p,q$ and $k>k'>p,q$. Figures 11(a) and 11(b) show the separate contributions to the energy and enstrophy flux for $k'=50$ in the enstrophy inertial range. Clearly, the enstrophy flux here (the area under the curve) is due almost entirely to triads for which $k\gtrsim k'$. The energy flux has equal but opposite contributions from $\Pi^{E+}_{k'}$ and $\Pi^{E-}_{k'}$, resulting in no *net* energy flux. To determine which triads are responsible for the major contributions to the flux, we must look at the p (or q) dependence of $\Pi^E_{k'k}$ (which is qualitatively the same as $\Pi^Z_{k'k}$ since they differ by a factor of k^2) as in Figs. 11(c) and 11(d). Thus we arrive at the following scenario for enstrophy inertial range fluxes: The important triad interactions are nonlocal, and the enstrophy flux through k' is primarily due to triads with $k'\approx k>p\gg q$, while the energy flux has the additional contribution from $p,\ q>k'\gg k$ which may be thought of as "backscatter" from high wave numbers.

Consider a simple schematic model of the process as seen in Fig. 12. Assume that the energy transfer function T_{kpq} can be approximated as a simple step function in p

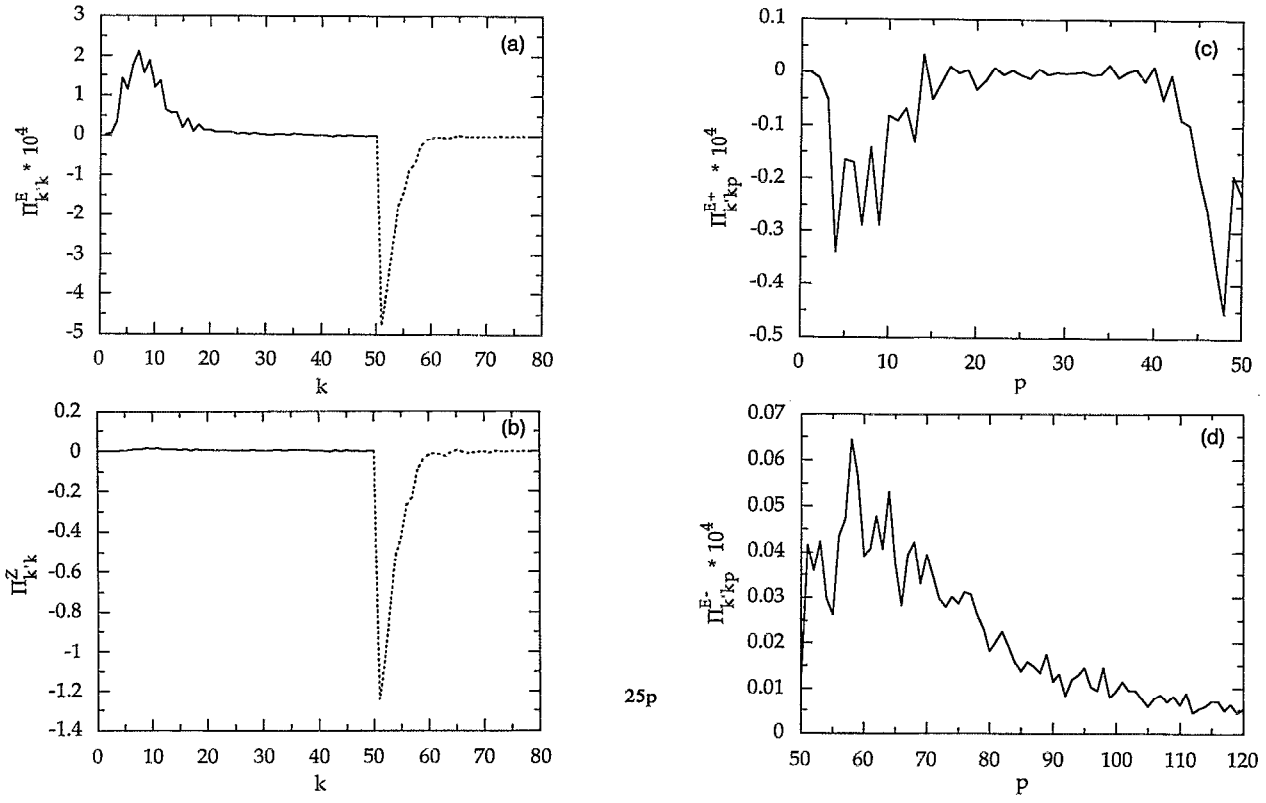

FIG. 11. Contributions to the enstrophy inertial range flux for $k'=50$. (a) The energy flux contributions $\Pi^{E+}_{k'k}$ (dashed curve) and $\Pi^{E-}_{k'k}$ (solid curve). (b) The enstrophy flux contributions $\Pi^{Z+}_{k'k}$ (dashed curve) and $\Pi^{Z-}_{k'k}$ (solid curve). (c) The p dependence of $\Pi^{E+}_{k'k}$ for $k=52$. The contribution from small p is due to the symmetry in p and q and the integral over p gives the value of $\Pi^{E+}_{k'k}$ for $k=52$. (d) The p dependence of $\Pi^{E-}_{k'k}$ for $k=8$. The integral over p gives the value of $\Pi^{E-}_{k'k}$ for $k=8$.

space with constant (independent of k) width Δ and amplitude $\hat{T}_k$. Also assume that this shape is independent of q, and that $\hat{T}_k$ is zero for $q>\Delta$. The value of Δ is of the order of 10, so this represents transfer due to triads with $k\approx p\gg q$. A plot of S_{kpq} [as in Fig. 4(a)] as defined here would have Δ different curves that all lie on top of each other.

Replacing the sums in (25) and (26) with integrals we can solve for the inertial range fluxes. First solve for the energy flux:

$$\Pi^{E+}_{k'} = \int_{k'}^{k'+\Delta} dk \int_{k-\Delta}^{k'} dp \int_0^{\Delta} \hat{T}_k \, dq$$
$$= \Delta \int_{k'}^{k'+\Delta} \hat{T}_k (k'+\Delta-k) dk. \tag{27}$$

We know from simulations that T_{kp} falls off approximately as k^{-2}, so let $\hat{T}_k \equiv \hat{S}/k^2$, and after assuming $\Delta \ll k'$ we obtain

$$\Pi^{E+}_{k'} \sim \hat{S} \frac{\Delta^3}{k'^2}. \tag{28}$$

Triads with $p\approx q\gg k$ contribute to the backscatter flux;

$$\Pi^{E-}_{k'} = \int_0^{\Delta} dk \int_{k'}^{\infty} dp \int_p^{p+\Delta} T_{kpq} \, dq. \tag{29}$$

For $p\gg k$, we can use $T_{kpq}\approx -(2k/p)T_{pqk}$, so we find

$$\Pi^{E-}_{k'} \sim -\hat{S} \frac{\Delta^3}{k'^2}. \tag{30}$$

Thus we see that $\Pi^{E+}_{k'}$ and $\Pi^{E-}_{k'}$ are of the same order, but opposite in sign, so we get no net energy flux. This shows that even though each individual triad that contributes to $\Pi^{E-}_{k'}$ sends a relatively small amount of energy past k' to small wave numbers, the sum of the energy from all rele-

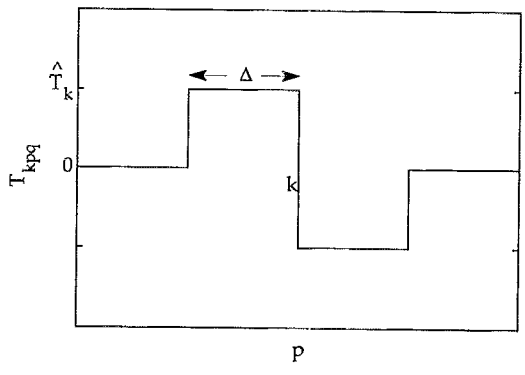

FIG. 12. Schematic of an idealized transfer function.

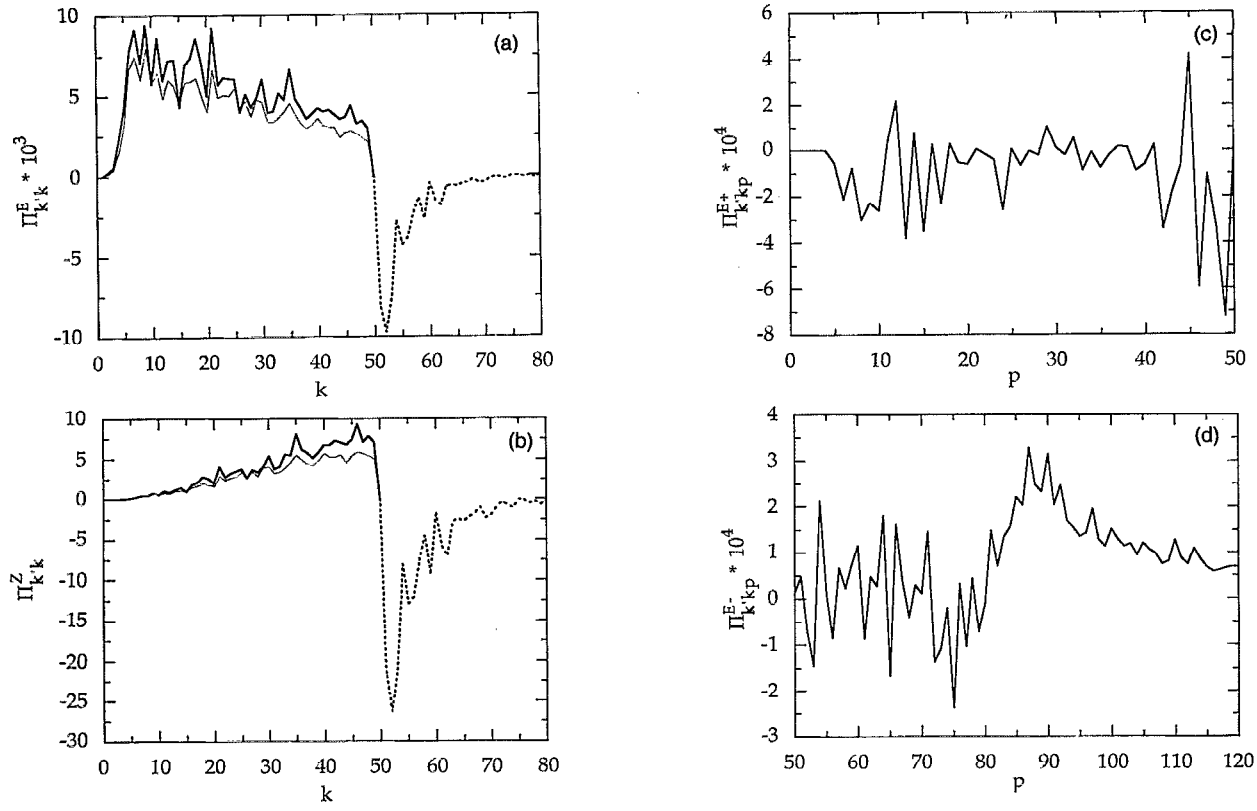

FIG. 13. Contributions to the energy inertial range flux for $k'=50$. (a) The energy flux contributions $\Pi^{E+}_{k'k}$ (dashed curve) and $\Pi^{E-}_{k'k}$ (thick solid curve). The thin solid curve is the contribution to $\Pi^{E-}_{k'k}$ for $p>k_f$, where $k_f=80$ defines the lower end of the forcing range. (b) The enstrophy flux contributions $\Pi^{Z+}_{k'k}$ (dashed curve) and $\Pi^{Z-}_{k'k}$ (thick solid curve). The thin solid curve has the same meaning as in (a). (c) The p dependence of $\Pi^{E+}_{k'k}$ for $k=55$. (d) The p dependence of $\Pi^{E-}_{k'k}$ for $k=10$.

vant triads is just enough to balance $\Pi^{E+}_{k'}$. (Note that there are many more triads contributing to $\Pi^{E-}_{k'}$ than $\Pi^{E+}_{k'}$.)

We may solve for the enstrophy flux in the same way as the energy flux to obtain

$$\Pi^{Z+}_{k'} \sim \hat{S}\Delta^3; \quad \Pi^{Z-}_{k'} \sim -\hat{S}\Delta^3\left(\frac{\Delta}{k'}\right)^2. \tag{31}$$

Since $k' \gg \Delta$, the enstrophy flux is dominated by $\Pi^{Z+}_{k'}$, meaning that it is the exchange of enstrophy between wave numbers of similar length and orientation that is responsible for essentially all of the inertial range flux of enstrophy, unlike the energy flux which has an important contribution from modes of very different length and orientation (i.e., between the smallest and middle modes).

Investigation of the transfer functions in the energy inertial range (Sec. IV) showed transfer to both large and small scales which must combine to give an energy flux to large scales. Contributions to the energy inertial range fluxes at $k'=50$ can be seen in Figs. 13(a) and 13(b). As in the enstrophy inertial range, triads with $k' \approx k > p \gg q$ are associated with energy and enstrophy flux to small scales. Whereas this was the only important type of triad contributing to enstrophy flux in the enstrophy inertial range, now there is an equal and opposite contribution from $\Pi^{Z-}_{k'}$ resulting in no net enstrophy flux. The energy flux now has a large contribution from $\Pi^{E-}_{k'}$ that more than cancels the energy flux to small scales associated with $\Pi^{E+}_{k'}$, resulting in a net flux of energy to large scales. To discover which triads are important in the energy cascade, consider the p dependence of $\Pi^{E}_{k'k}$. Typical contributions to $\Pi^{E+}_{k'k}$ [Fig. 13(c)] are similar to what was found in the enstrophy inertial range. However, there is a noticeable difference in the p dependence of $\Pi^{E-}_{k'k}$ [Fig. 13(d)]. Whereas in the enstrophy inertial range the important triads have $p \gtrsim k' \gg k$, here the important contributions come from $p \gtrsim k_f \gg k$ [Fig. 11(c)]. That is to say, the important triads contributing to the inverse energy cascade have one small member near the spectral peak, and two members at higher wave number, with at least one in the enstrophy inertial range above the forcing range. Contributions from $k'<p<k_f$ are also typically positive, but far less regular.

It seems intuitive to suppose that the importance of interactions involving $p>k_f$ contributing to the flux past k' would become unimportant as $(k_f-k') \to \infty$. This tendency appears to hold in a higher resolution simulation with a longer inertial range where k' is held fixed but k_f is increased[23] [Fig. 14(a)]. However, there continue to be significant contributions to $\Pi^{E-}_{k'k}$ from $p>k_f$ [Fig. 14(b)]. The contributions from $k'<p<k_f$ are now slightly more obviously positive, but remain very irregular. There are clearly different mechanisms involved with the transfer in these two regions. Perhaps the intermediate range (i.e.,

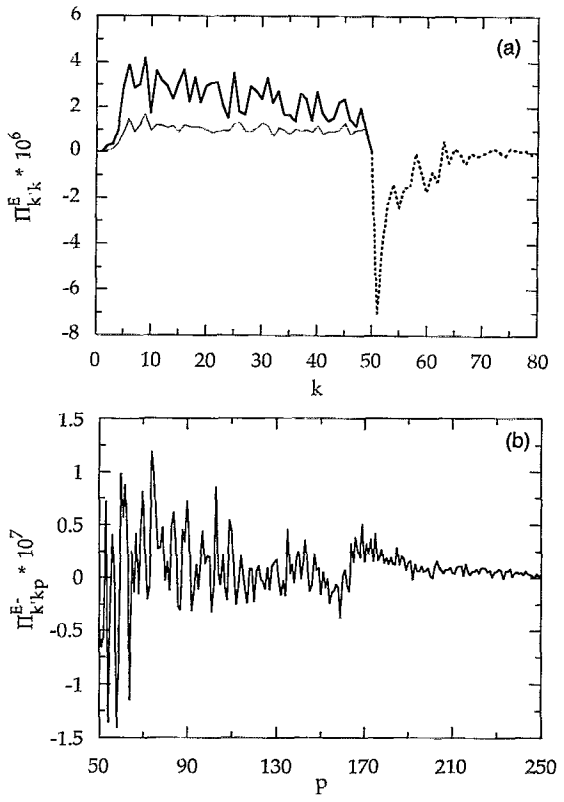

FIG. 14. Contributions to the energy inertial range flux for $k'=50$ from a high resolution run with forcing in the range $160\leqslant k\leqslant 165$. (a) $\Pi^{E+}_{k'k}$ (dashed curve) and $\Pi^{E-}_{k'k}$ (thick solid curve). The thin solid curve is the contribution to $\Pi^{E-}_{k'k}$ for $p>k_f$, where $k_f=160$ defines the lower end of the forcing range. (b) The p dependence of $\Pi^{E-}_{k'k}$ for $k=10$.

$k'<p<k_f$), being quite erratic, has some relationship to vortex merger events. In any event, for a sufficiently long inertial range, contributions from this range will likely dominate, and it will be important to investigate the mechanisms by which this transfer occurs.

VII. SUMMARY AND DISCUSSION

Inertial range transfer functions and flux have been examined with a view to understanding how well the classical phenomenological theories of two-dimensional turbulence perform, and what factors may contribute to their successes and failures. We have concentrated on an analysis in spectral space, although a discussion in physical space may be more of an appropriate setting to examine the role of coherent vortices and the like.[10]

It is clear for the enstrophy inertial range that important triad interactions (those that have high transfer rates) tend to be very nonlocal in the sense that two of the three legs are much longer than the third. For the enstrophy cascade, this may be associated with the usual physical picture of vorticity filaments being elongated and forced closer together by a large-scale flow. No matter what the scale of the filaments, in the simulations analyzed here the significant straining scale is in the vicinity of the spectral peak of energy. This is consistent with the heuristic arguments based on (1) for spectra steeper than k^{-3}. In such triad interactions, the largest scale receives a negligible amount of enstrophy, so one may consider the transfer to be *local* in the sense that enstrophy is transferred only between the two modes of similar size and orientation. Similarly, the enstrophy flux may be considered local since the flux at k' may be determined by contributions from $k\gtrsim k'$. However, the triad interactions are manifestly *nonlocal.* Furthermore, they are not similar in shape at all scales: for a given integration, the important triads at all scales contain a member close to the spectral peak. Thus, even though enstrophy transfer is local in the sense used above, the influence of the large scales may be communicated directly to all scales. Thus, the notion of a chaotic cascade, in which information about the forcing scales is gradually lost as enstrophy is transferred in small steps to the small scales, would appear to be invalid. Still higher resolution simulations of two-dimensional turbulence could of course modify this conclusion.

Energy transfer in the enstrophy inertial range is a little more involved. There is a local component of the energy transfer to small scales that is associated with the downscale enstrophy transfer. However, a significant amount of energy is also transferred to the smallest member of the triad, referred to as "backscatter." Backscatter may be thought of as a *nonlocal* process, since a small wave number is receiving energy directly from a much larger wave number. The backscatter, when integrated over all appropriate triads, produces a nonlocal energy flux which cancels the local component, resulting in no net energy flux in the enstrophy inertial range. It is interesting to note that although approximately 70% of the possible triad interactions for a given k transfer more energy between the smallest and middle wave numbers than between the middle and largest,[24] most of the important interactions fall in the 30% that transfer more energy between the two larger members of the triad.

Transfer in the energy inertial range appears to be quite complex. One aspect of the transfer is similar to the enstrophy inertial range, that is, energy and enstrophy are transferred to smaller scales via elongated triads. Here, the same physical mechanism at work in the enstrophy inertial range (straining of vorticity filaments) appears to be present, though it may be less efficient and result from a somewhat wider range of triads. This type of transfer is again responsible for a flux of energy and enstrophy toward small scales. Backscatter again provides a nonlocal flux directed toward large scales from very nonlocal interactions, though it differs from the enstrophy inertial range. A significant portion of the energy flux comes from nonlocal triads with the large members in the enstrophy inertial range in and above the forcing range and is large enough to more than balance the downscale contribution, resulting in a net flux of energy to large scales, as expected. In contrast with the enstrophy inertial range, the backscatter does bring some enstrophy back to large scales, and when integrated over all appropriate triads, produces a flux that cancels the local contribution, resulting in no net enstrophy flux in the energy inertial range.

The notion of energy "cascade" in the energy inertial

range also would seem to have limited validity, in that the small scales inject energy directly (i.e., via a nonlocal interaction) into the large-scale flow. This is consistent with the conclusion reached by examining the vorticity field in physical space from simulations forced at high wave numbers: that is, the energy flux is not primarily due to vortex mergers, since vortices are observed to be present at scales only slightly larger than the forcing scale. While merger events may play a part in the energy flux, a clear physical mechanism for the inverse "cascade" remains to be clarified.

ACKNOWLEDGMENTS

The authors would like to thank Piero Olla for many helpful discussions.

We would like to thank the Fluid Dynamics group and the Institute for Geophysics and Planetary Physics at Los Alamos National Laboratory for support. This work was also supported by the National Science Foundation (Grant No. ATM 8914004) and the Office of Naval Research (Grant No. N00014-90-J-1618). More details of this work may be found in Ref. 25.

APPENDIX: IMPLICATIONS FOR SUBGRID-SCALE MODELING

In the simulations described in this paper, we have modeled the effect of the subgrid scale with a high-order diffusion which keeps enstrophy from building up at the smallest resolved scale. In this sense, our simulations are not direct but are "large eddy simulations." Such a scheme appears *ad hoc*, but is very useful for numerical simulations. Here we examine the appropriateness of such a description based on the transfer functions described in the body of this paper.

The premise for this discussion of subgrid-scale modeling is schematized in Fig. 15. Consider an extremely long enstrophy inertial range that has evolved to a statistically steady state, thus, the area under the S_{kp} curve [which we assume has the shape seen in, for example, Fig. 2(a)] must be zero for any k. If the system is suddenly truncated, and the maximum resolved wave number (denoted by the dotted line in Fig. 15) is too close to k, the shaded part of the S_{kp} curve is no longer resolved. This makes the area under the S_{kp} curve positive, which in turn increases (artificially) the enstrophy in mode k. Unless dissipation is added, this "piling up" of enstrophy continues until the spurious small-scale effects dominate the flow.

If we assume that S_{kpq} has the same shape for all of the unresolved scales as for the resolved scales, then the ideal diffusive subgrid-scale model would simply dispose of the excess enstrophy that should be transferred out to modes that are not explicitly resolved. That is, the dissipation rate should be equal to the area of the shaded region in Fig. 15,

$$\dot{D}'_k \equiv \sum_{p=k_{\max}}^{\infty} S_{kp}. \tag{A1}$$

Figure 16(a) shows a comparison of $\dot{D}'_k$ and the true dissipation rate $\dot{D}_k = \nu_9 k^{18} E_k$. Here $\dot{D}'_k$ was calculated using

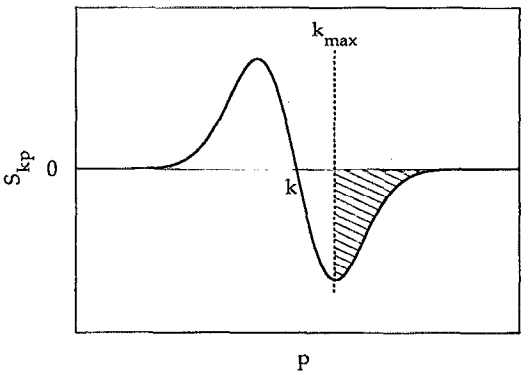

FIG. 15. Schematic of the premise for subgrid-scale modeling.

S_{kp} for $k=70$ as representative of S_{kp} for all k in the inertial range, which we have seen is a good approximation [see Fig. 2(b)]. We are particularly interested in the shape of each curve, that is, at what wave number does dissipation become important? It is clear that, even with a very high-order diffusion, dissipation ($\dot{D}_k$) becomes important in this simulation (around $k=95$) earlier than it needs to be since $\dot{D}'_k$ does not in fact become significant until approximately

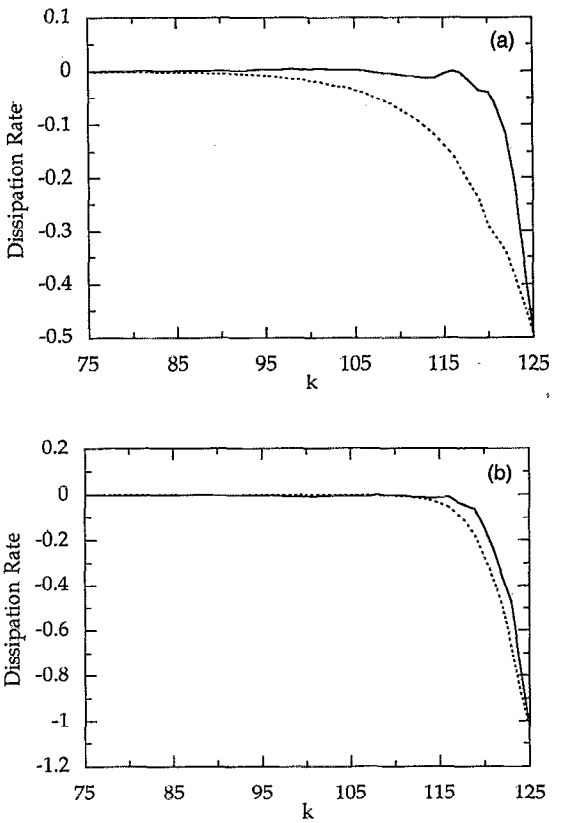

FIG. 16. The true dissipation rate $\dot{D}(k)$ (dashed curve) and the transfer deficit $\dot{D}'(k)$ (solid curve). $\dot{D}'(k)$ has been rescaled so that its maximum is the same as for $\dot{D}(k)$. (a) The diffusion operator is given by $\nabla^{18}\psi$. (b) The diffusion operator is given by $\nabla^{48}\psi$. Other model parameters are the same as in (a).

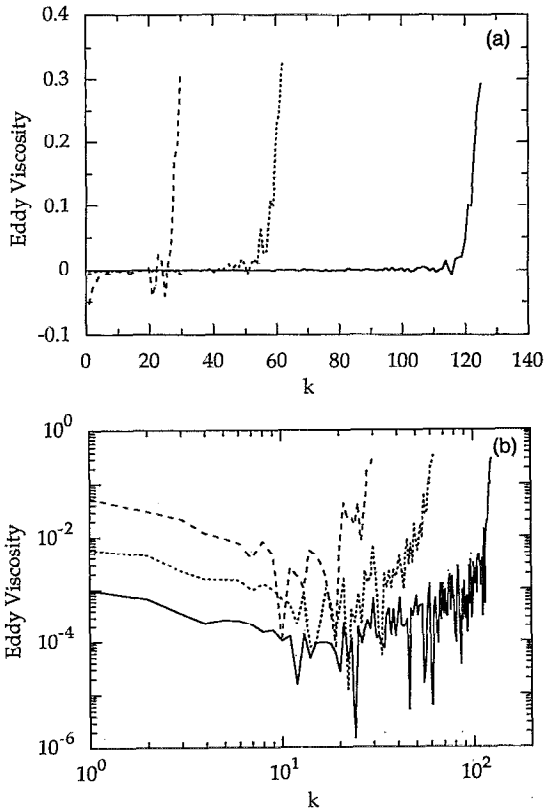

FIG. 17. (a) The eddy viscosity calculated by truncating a 512^2 simulation at $k_t=128$ (solid curve), $k_t=64$ (short dashed curve), and $k_t=32$ (long dashed curve). Note the negative values at low k particularly apparent for $k_t=32$. (b) The same curves as in (a) except on a log–log scale. Negative values at low k have their absolute value plotted.

$k=110$. This implies that one could choose an even higher-order diffusion that would be an even closer approximation to the inviscid dynamics.

We can use simple scaling to estimate the order of diffusion necessary to produce a curve similar to $\dot{D}'_k$ in Fig. 16(a). Defining k_ν as the scale at which the diffusion time scale ($t_\nu \approx 1/\nu k^{2n}$) and dynamical time scale ($t_\xi \approx 1/\xi_{\rm rms}$) are equal, we find $k_\nu \approx \gamma' k_{\rm max}$, where $\gamma' = \gamma^{-1/2n} k_{\rm max}^{-1/n}$ and γ is an order one tuning factor and n is the power of ∇^2. As reference, this expression gives $k_\nu \approx 90$ for the simulation shown in Fig. 16(a). If we want to choose a diffusion that would give $k_\nu \approx 110$ as suggested by $\dot{D}'_k$, a value of $n \approx 24$ would be necessary, meaning the diffusion operator would be $D_k = \nu\nabla^{48}\psi$. Figure 16(b) shows a simulation like the one in Fig. 16(a) but uses $\nabla^{48}\psi$ for diffusion. Even this high of an order diffusivity is unable to move the dissipation wave number as high as transfer arguments would suggest. Attempts to use even higher-order diffusion to increase the dissipation wave number were unsuccessful, in part due to the fact that having too steep of a drop-off in the dissipation range is similar to simply truncating the system further, resulting in the kind of spurious enstrophy buildup that the subgrid-scale model is introduced to alleviate.

Another way of looking at this problem is in terms of a wave-number-dependent eddy viscosity coefficient,[26] $D(k)=\nu_k^e \nabla^2 \xi$, which models the transfer into resolved scales from unresolved scales. Note that the eddy coefficient ν_k^e may be negative, representing transfer *into* a given mode. In practice, we can determine the form of ν_k^e by truncating the resolution of a given simulation and measuring the difference in the transfer as a function of k compared to the full resolution. If we have a simulation with maximum resolved wave number $k_{\rm max}$, we truncate the system at $k=k_t$ by setting to zero all modes with $k_t<k<k_{\rm max}$, then the eddy viscosity[27] may be defined as

$$\nu_k^e = \frac{[J_k(\psi,\xi) - J_k(\tilde{\psi},\tilde{\xi})]\psi_k^*}{k^4 \psi_k \psi_k^*}, \tag{A2}$$

where $\tilde{\psi}$ and $\tilde{\xi}$ are the truncated streamfunction and vorticity. Figure 17 shows the eddy viscosity calculated from a high resolution run ($k_{\rm max}=256$) with truncations at $k_t=128$, 64, and 32. Note the similarity of the $k_t=128$ curve with $\dot{D}'(k)$ in Fig. 16.

Summarizing, a subgrid-scale parametrization for two-dimensional turbulence should substantially affect only those wave numbers close to the truncation wave number—typically those within a distance Δ from the truncation, where Δ is of order the wave number of the spectral peak. In a spectral simulation this may be most easily implemented with a high-order diffusion operator. In limited area and grid-point models the ease of implementation of boundary conditions will also be an important consideration in the particular form chosen for the filter.

[1] R. H. Kraichnan, "Inertial ranges in two-dimensional turbulence," Phys. Fluids **10**, 1417 (1967).

[2] J. C. McWilliams, "The emergence of coherent vortices in turbulent flow," J. Fluid Mech. **146**, 21 (1984).

[3] B. Legras, P. Santangelo, and R. Benzi, "High resolution numerical experiments for forced two-dimensional turbulence," Europhys. Lett. **5**, 37 (1988).

[4] M. E. Maltrud and G. K. Vallis, "Energy spectra and coherent structures in forced two-dimensional and beta-plane turbulence," J. Fluid Mech. **228**, 321 (1991).

[5] U. Frisch and P.-L. Sulem, "Numerical simulation of the inverse cascade in two-dimensional turbulence," Phys. Fluids **27**, 1921 (1984).

[6] G. K. Vallis, "Problems and phenomenology in two-dimensional turbulence," in *Nonlinear Phenomena in the Atmospheric and Oceanic Sciences*, edited by G. Carnevale and R. Pierrehumbert (Springer-Verlag, Berlin, 1992), pp. 1–25.

[7] R. H. Kraichnan, "Inertial-range transfer in two- and three-dimensional turbulence," J. Fluid Mech. **47**, 525 (1971).

[8] C. Basdevant, M. Lesieur, and R. Sadourny, "Subgrid-scale modeling of enstrophy transfer in two-dimensional turbulence," J. Atmos. Sci. **35**, 1028 (1978).

[9] K. Ohkitani, "Nonlocality in a forced two-dimensional turbulence," Phys. Fluids A **2**, 1529 (1990).

[10] K. Ohkitani, "Wave-number space dynamics of enstrophy cascade in a forced two-dimensional turbulence," Phys. Fluids A **3**, 1598 (1991).

[11] J. Weiss, "The dynamics of enstrophy transfer in two-dimensional hydrodynamics," Physica D **48**, 273 (1991).

[12] J. A. Domaradzki and R. S. Rogallo, "Local energy transfer and nonlocal interactions in homogeneous isotropic turbulence," Phys. Fluids A **2**, 413 (1990).

[13] Smyth has shown that using the nonsymmetric transfer function can be very useful in studying turbulence in the presence of a nonzero mean flow. W. D. Smyth, "Spectral transfers in two-dimensional anisotropic flow," Phys. Fluids A **4**, 340 (1992).

[14] G. S. Patterson and S. A. Orszag, "Spectral calculation of isotropic turbulence: Efficient removal of aliasing interaction," Phys. Fluids **14**, 2538 (1971).

[15]A. J. Robert, "The integration of a low-order spectral form of the primitive meteorological equations," J. Meteor. Soc. Jpn. Ser. 2 **44**, 237 (1966).
[16]A. Pouquet, M. Lesieur, J. C. Andre, and C. Basdevant, "Evolution of high Reynolds number two-dimensional turbulence," J. Fluid Mech. **72**, 305 (1975).
[17]J. A. Domaradzki, "Analysis of energy transfer in direct numerical simulations of isotropic turbulence," Phys. Fluids **31**, 2747 (1988).
[18]S. A. Orszag, "Analytical theories of turbulence," J. Fluid Mech. **41**, 363 (1970).
[19]C. E. Leith, "Atmospheric predictability and two-dimensional turbulence," J. Atmos. Sci. **28**, 145 (1971).
[20]J. R. Herring and J. C. McWilliams, "Comparison of direct numerical simulation of two-dimensional turbulence with two-point closure: The effects of intermittency," J. Fluid Mech. **153**, 229 (1985).
[21]Transfer functions from the closure will have wave-number dependencies in parentheses to distinguish them from the subscripted functions calculated by the direct simulations.
[22]This error is likely exaggerated by the fact that the model is not in an EDQNM steady state.
[23]The same tendency is seen if k_f is held fixed and k' is decreased.
[24]P. Merilees and H. Warn, "On energy and enstrophy exchanges in two-dimensional nondivergent flow," J. Fluid Mech. **69**, 625 (1975).
[25]M. E. Maltrud, "Structures, spectra, and inertial range transfer in two-dimensional and betaplane turbulence," Ph.D. thesis, University of California, San Diego, 1992.
[26]R. H. Kraichnan, "Eddy viscosity in two and three dimensions," J. Atmos. Sci. **33**, 1521 (1976).
[27]G. K. Vallis and B. Hua, "Eddy viscosity of the anticipated potential vorticity method," J. Atmos. Sci. **45**, 617 (1988).